# Comparison of one-dimensional turbulence and direct numerical simulations of soot formation and transport in a nonpremixed ethylene jet flame

David O. Lignell[a,1], Garrison C. Fredline[a], Adam D. Lewis[a]

[a] *350 CB, Brigham Young University, Provo, UT 84602, USA*

**Abstract**

Accurate models of soot formation in turbulent flames are important for correctly predicting and simulating flames and fires. Modeling soot formation and transport is challenging due to the complex chemical formation processes, and differential diffusion of soot relative to a flame. Direct numerical simulations (DNS) have highlighted the importance of such transport on soot concentrations, however DNS is computationally expensive. The one-dimensional turbulence (ODT) model is able resolve a full range of length and timescales and solves the evolution of diffusive and reactive scalars in the natural physical coordinate. We present results of soot formation in ODT and compare the model to simulation results from DNS in a temporally-evolving planar ethylene jet flame where the same transport, thermodynamic, and kinetic models are applied. Good agreement is found for the jet evolution in terms of the mixture fraction profiles. Conditional soot statistics (mean and fluctuations) are presented, along with joint soot-mixture fraction PDFs that illustrate the location and motion of soot in the mixture fraction coordinate. Good qualitative agreement between the models is found and the soot behavior is similar. While the ODT cannot capture three-dimensional flow structures, the ODT simulations are less computationally expensive than the DNS suggesting its use in conjunction with DNS for parametric study, model validation, and investigation at parameter ranges not currently available to DNS.

*Keywords:* Soot, ODT, DNS, turbulent, nonpremixed flame

## 1. Introduction

Soot is an important component of most nonpremixed flames and fires. Soot radiation affects flame temperatures, impacting, for instance, flame spread and industrial radiative heat transfer. Large fires exhibit increases in radiative intensity with size, but when smoke breaks through the fire, smoke shielding can reduce this intensity. Emission of soot from flames results in fine carbonaceous particles that contribute to air pollution, and are a known health hazard contributing to lung diseases, such as asthma, bronchitis, and other problems [1].

Modeling soot formation and transport is a challenging problem. Soot formation involves complex formation chemistry based on large aromatic hydrocarbons. Soot is a particle phase with an evolving size and composition distribution, which grows to form primary particles that aggregate into chain-like structures [2]. The low diffusivity of soot results in very fine soot filaments due to turbulent stretching and folding. This increases computational costs of direct numerical simulations (DNS) that resolve all turbulent scales. Similarly, the low diffusivity implies differential diffusion between soot and gaseous species so that soot is transported relative to flame surfaces largely by the relative velocity difference between convection and the stoichiometric (flame) isosurface [3]. The transport of soot relative to a flame will affect the temperature and composition environment of the soot, impacting soot formation, and radiation. The differential diffusion complicates LES modeling since subgrid differential diffusion should be accounted for in combustion models (but is often neglected). The differential diffusion coupled with longer formation timescales results in the well-known lack of a state relationship between soot and the mixture fraction [4].

These challenges, among others, motivate detailed study of soot formation in turbulent combustion. DNS is a useful tool for such investigation. A few recent DNS have been performed of soot formation in turbulent flames. These include a two-dimensional study with one-step ethylene chemistry in an opposed jet configuration by Yoo et al. (2007) [5]. Lignell et al. [3] simulated a two-dimensional flame with detailed chemistry and a semi-empirical soot model. See also Bisetti et al. [6] who used a detailed soot model. Lignell et al. [7] simulated a three-dimensional DNS with soot formation using a similar model in a turbulent ethylene jet flame. Attili et al. [8] performed DNS of soot formation in nonpremixed n-heptane flames.

While DNS provides detailed spatial and temporal information on composition, temperature, velocity, and soot fields, the simulations are limited to relatively short run times and lower Reynolds numbers compared to practical

*Corresponding author

*Email address:* davidlignell@byu.edu (David O. Lignell)

[1] Phone: (801) 422-1772

flames and fires. The high computational cost of DNS also increases processing time and limits the number of parametric simulations that can be performed.

The one-dimensional turbulence (ODT) model [9] solves unsteady transport equations for mass, momentum, energy, and reacting scalars in one dimension. ODT resolves diffusive mixing and flame interactions in the natural physical coordinate, but models turbulent advection through stochastic mapping processes that occur concurrently with the scalar evolution equations and reproduce key aspects of turbulent mixing. ODT is limited to geometrically simple flows and is best suited boundary-layer flows, such as jets, with a dominant direction of mean shear. Boundary layer flows are commonly studied and practically important. Three-dimensional simulations have been performed with ODT by constructing grids of interacting ODT lines that could permit study of more complex flows [10]. The model has been successfully applied to a wide range of reacting and nonreacting flows [11]. ODT is computationally efficient compared to DNS because it is one-dimensional. Several ODT simulations have been performed of combustion including comparison to experiments of jet flames [12], and investigation of flame extinction and reignition [13]. ODT has been compared directly to DNS data for application to flame extinction and reignition in syngas flames [14], and ethylene flames [15]. Ricks et al. (2010) [16] simulated soot evolution in buoyant pool fires, and Zimberg et al. (1998) simulated soot formation using the linear eddy model (LEM) [17], which is a precursor to ODT.

Here, we compare the ODT model directly to three-dimensional DNS [7] of soot formation in a turbulent, planar, temporal ethylene jet flame. This comparison has the advantage of using the same combustion, transport, and soot models in a compatible configuration. Hence, the accuracy of the ODT model may be assessed without complicating uncertainties that often arise in comparing ODT to experimental data, such as consistency of boundary conditions, spatial versus temporal evolution, planar versus cylindrical geometry, and limited data for comparison. Successful comparisons of ODT and DNS will lend confidence to, and quantify limitations of, using ODT directly to study turbulent soot formation, preferably in conjunction with DNS, LES, and experiments to develop and validate more accurate models of soot formation in turbulent flames. We emphasize however, that ODT is a model and cannot replace DNS. In addition, we note that turbulent soot formation is a complex process; and while the ODT and DNS are compared using the same models, the model used in the DNS is not a *true* solution. Continued investigation is needed (including experimental validation) with more detailed soot models in a variety of turbulent flow environments that excercise a wide range of time and length scales, soot-temperature-mixture fraction histories, and radiative effects.

## 2. Numerical methods

The flow configuration and DNS were described in Lignell et al. [7]. Here a summary description is given, along with a description of the ODT model and simulations.

The flow configuration is a temporally-evolving, planar, ethylene jet flame. Initially, a planar slab of fuel is surrounded by oxidizer. The initial fuel jet width is $H$=1.8 mm, and the streamwise velocity difference between the fuel and oxidizer is $U$=82 m/s, yielding a jet Reynolds number of 3700. Due to this relatively low Reynolds number, the jet is essentially in a transitionally turbulent regime. The fuel and oxidizer streams are 25.46% ethylene and 26.41% oxygen, respectively, with the balance nitrogen, giving a stoichiometric mixture fraction of $\xi_{st} = 0.25$. The streams are both preheated to 550 K. The flames are initialized by mapping a consistent steady laminar flamelet profile to the initial mixture fraction field. The flow is statistically one-dimensional with mean gradients in the cross-stream direction. The simulation dimensions are $16H$, $11H$, and $6H$ in the streamwise, cross-stream, and spanwise directions, respectively. The computational grid size for the DNS is 30 $\mu m$, and the simulation is run for 50 jet times ($\tau_j = H/U$). Boundary conditions are periodic in the streamwise and spanwise directions, and non-reflecting outflow in the cross-stream direction.

The DNS was performed using S3D developed at Sandia National Laboratories [18]. S3D solves the compressible, reacting, Navier-Stokes equations using an explicit fourth-order Runge-Kutta method for time integration. Spatial derivatives are approximated using eight-order finite difference approximations. A spatial filter is applied to remove aliasing errors. Chemkin [19] is used to compute thermodynamic quantities, and the Chemkin Transport [20] package is used to compute thermal conductivities, viscosities, and species diffusivities. Mixture averaged effective diffusivities are used for species diffusion fluxes.

The combustion chemistry is described with a reduced ethylene mechanism consisting of 19 transported species and 10 quasi-steady-state species, with 167 reactions [3]. The method of moments is used to represent the soot particle size distribution. The first three mass moments of the size distribution are transported [21]. The semi-empirical model of Leung et al. [22] is used to describe the soot nucleation, growth, coagulation, and oxidation processes. The moment transport equations are closed assuming a lognormal size distribution. Soot transport occurs by convection and thermophoretic diffusion. In the DNS, Brownian diffusion is also included, but is small compared to the other transport processes.

ODT solves unsteady transport equations for mass, momentum, energy and chemical species on a one-dimensional domain. The domain is aligned with the inhomogeneous cross-stream direction in the temporal jet configuration. Turbulent advection is modeled by the occurence of instantaneous eddy events of a given size and location that occur concurrently with the solution of the transport equa-

tions. A given eddy event is implemented as a triplet map by replacing all solution profiles in the eddy region with three copies of each profile, each spatially compressed by a factor of three, lined up to span the eddy region, and the center copy is spatially mirrored. The resulting profiles are continuous and fully conservative, with increases in local gradients and strain [17, 9]. Eddy sizes, locations, and frequencies are computed stochastically, based on the computed momentum fields in a manner consistent with turbulent scaling laws. Details can be found in Ref. [23]. The model includes an eddy rate parameter $C$, a viscous penalty parameter $Z$, and a large eddy suppression parameter $\beta$ that requires $\beta\tau_e < t$, that is $\beta$ times the eddy timescale should be less than the elapsed simulation time. Here, $C = 8$, $Z = 0$, and $\beta = 1$ are used. These parameters were chosen to give reasonable simultaneous agreement for the jet evolution, scalar dissipation, and soot concentrations, described below.

The ODT code is written in C++ and solves and solves the unsteady transport equations using a Lagrangian finite volume formulation on a dynamically adaptive mesh. A low-Mach formulation is assumed in the solution approach. Transport equations for a given grid cell are of the form

$$\frac{d\phi}{dt} = -\frac{1}{\rho\Delta x}(j_{\phi,e} - j_{\phi,w}) + S_\phi, \tag{1}$$

where $\phi$ is a transported scalar per unit mass, $S$ is the chemical and soot source term [3, 21], and $j$ is the diffusion flux, where subscripts $e$ and $w$ denote the east and west faces of a grid cell of size $\Delta x$. Equations are solved for $\phi = u_k$, $h$, $Y_k$, $M_i/\rho$, that is, velocity components, enthalpy, gaseous species mass fractions, and soot moments per unit mass, respectively. In the Lagrangian formulation, grid cell sizes are adjusted so that $\rho\Delta x$ is constant. The following constitutive relations are used for momentum, enthalpy, gaseous species, and soot moment fluxes, respectively,

$$\tau_k = -\mu\frac{du_k}{dx}, \tag{2}$$

$$q = -\lambda\frac{dT}{dx} + \sum_k h_k j_k, \tag{3}$$

$$j_k = -\frac{\rho Y_k D_k}{X_k}\frac{dX_k}{dx}, \tag{4}$$

$$j_i = -0.554\nu M_i\frac{d\ln T}{dx}. \tag{5}$$

Thermochemical and transport properties are computing using Cantera [24]. A first order explicit time integration with second order central differences on spatial derivatives is used. A total of 512 ODT realizations were computed to gather flow statistics. Adequate resolution was found with a minimum cell size of 19.8 $\mu$m. A grid resolution study was performed with the minimum allowable cell size at half and twice the above chosen value. The finer grid simulation also had double the grid resolution parameter so that nominally twice as many grid points were used to resolve scalar structures. No significant differences in results were found.

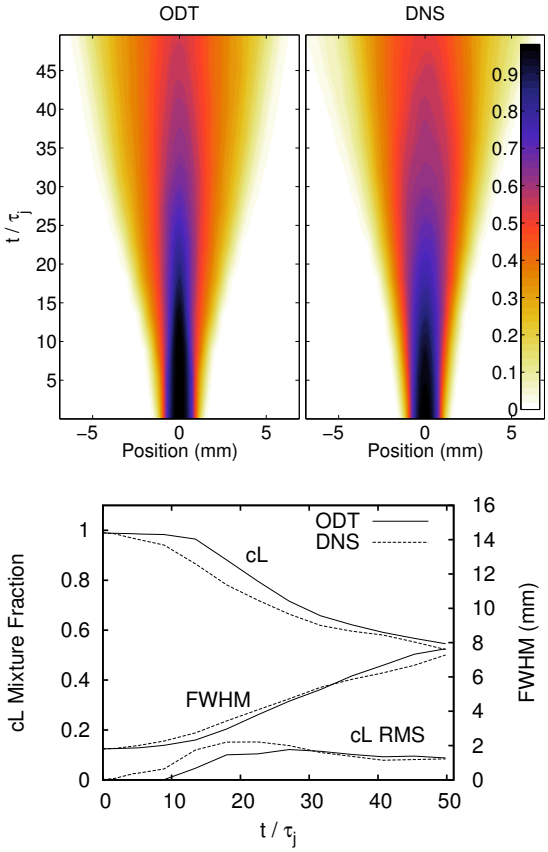


Figure 1: Top: mean mixture fraction profiles. Bottom: full width at half maximum (FWHM) mean mixture fraction along with mean and RMS centerline mixture fraction profiles.

The raw simulation costs were 1.5 million CPU-hours for the DNS, and 300 hours for the 512 ODT realizations. While direct comparison between the simulations is difficult, the costs roughly scale with the number of grid points, time steps, evaluation stages per time step in the ODE solver, and the inverse processor speed. These values are 660, 104680, 6, and 2.4 GHz, respectively for the DNS, and 460 (average), 36690 (average), 1, and 2.8 GHz, respectively per realization for the ODT. On this basis, the ODT is 175 times less expensive than the DNS. In addition, DNS costs scale roughly with $Re^3$ [25], but $Re^{3/2}$ for ODT, so that the cost of DNS relative to ODT increases with increasing $Re$.

## 3. Results

The jet evolution may be characterized by the evolution of the mean mixture fraction, shown in Fig. 1. Contours of the mixture versus cross-stream position and time are shown. These contours are summarized in the lower plot as the centerline mean and the full width at half maximum profiles. The centerline root mean square

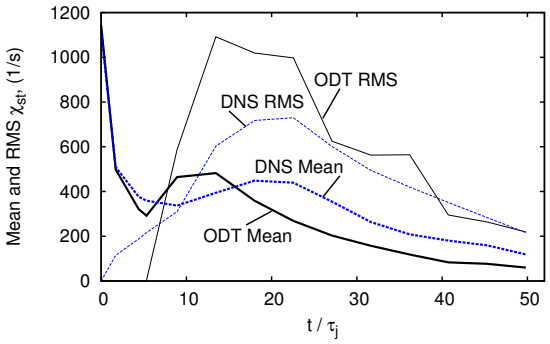


Figure 2: Stoichiometric scalar dissipation rate (mean and RMS) as a function of time for ODT and DNS simulations.

(RMS) mixture fraction fluctuation is also shown. The agreement between the DNS and the ODT is reasonably good. The ODT jet begins evolving somewhat later than the DNS. The centerline mixture fraction value is flat up to around 0.3 ms, then decays to 0.55, very close to the DNS. The FWHM profiles are very similar, though the ODT is slightly narrower early on. The centerline RMS mixture fraction is initially low for the ODT, then rises to about the same value as the DNS (though values off-center, not shown, are somewhat higher in the DNS than the ODT).

Figure 2 shows the evolution of the mean and RMS stoichiometric scalar dissipation rate in time. The mean dissipation begins relatively high at the initial condition corresponding to the gradient in the initial mixture fraction profile. The value deceases quickly with gaseous diffusion prior to the development of the jet turbulence. As the jet evolves, the scalar dissipation rate increases, reaches a peak, then decays. The RMS profile is initially zero, then rises to a peak and decays. The RMS scalar dissipation rate is higher than the mean after the initial decay. The ODT profiles are qualitatively the same as the DNS, and the peaks in the mean profiles are similar in magnitude, but the ODT peaks earlier in time, then decays decays faster than the DNS, whereas the ODT profile remains lower than the DNS after 0.35 ms. The ODT RMS profile is also somewhat higher than the DNS, and peaks slightly earlier, then decays to values close to the DNS. The differences in these profiles affect the corresponding soot profiles, discussed below.

Very close agreement of stoichiometric mean and RMS fluctuations was obtained between ODT and DNS for a flame extinction and reignition study in a similar temporal jet configuration [15], but at higher Reynolds number where ODT performs somewhat better. It may be possible to improve the present results through tighter tuning of the ODT parameters. In Ref. [15], sensitivity of results to ODT parameter variation was performed. As C decreases (lower eddy rate), the peak scalar dissipation rate decreases and moves to a later time. The $\beta$ parameter behaves opposite that of C, since smaller $\beta$ corresponds to larger eddies and higher mixing. Z sensitivity is much weaker, with lower Z causing somewhat lower scalar dissipation rate, and smaller eddies.

The conditional mean temperature profiles (not shown) are nearly identical between the ODT and the DNS, with peak mean values near stoichiometric at 2200 K. The peak conditional RMS profiles are qualitatively similar, but peak at 250 K for the ODT, and 150 K for the DNS.

Figure 3 shows representative lines of sight through the DNS simulation and representative profiles from single realizations for the ODT simulations. Temperature, mixture fraction, and scaled soot mass fraction are shown. The profiles will not be the same due to the chaotic and stochastic nature of the turbulence in the DNS and the eddy events in the ODT. Rather, the plots illustrate the similarities in the structures of the profiles shown. The temperature and mixture fraction profiles are much more diffuse than the corresponding soot profiles, which show very fine scale structure. The ability of ODT to capture the diffusive-reactive flow structure is emphasized in the figure.

The soot distribution in the mixture fraction coordinate is shown in Fig. 4 (and also later in Fig. 7). The figure shows plots of the conditional mean and RMS soot evolution in time. The stoichiometric (flame) mixture fraction is at $\xi = 0.25$ and the soot peaks at $\xi = 0.4$. Little soot exists lean of $\xi = 0.25$ where oxidation occurs, though there is a small amount of breakthrough, with the ODT exhibiting slightly more than the DNS. The soot concentration and corresponding RMS increase monotonically. The RMS magnitudes are similar to the magnitude of the soot concentration itself. The magnitude of the soot concentration, and hence the corresponding RMS is higher in the ODT than in the DNS. This is due to the somewhat lower scalar dissipation rate (favoring soot formation) of the ODT (Fig. 2) over the times shown in Fig. 4 where the soot concentration is rapidly increasing. In the high activation energy processes involved, the higher ODT RMS temperature fluctuations also contribute to increased ODT soot concentration.

The motion of the soot in the mixture fraction coordinate may be illustrated by examining the soot mass weighted PDFs of the mixture fraction $P_{\rho Y s}$. Physically $P_{\rho Y s}(\xi)d\xi$ represents the fraction of the soot mass between $\xi$ and $\xi + d\xi$, and is defined as

$$P_{\rho Y s} = \frac{\langle \rho Y_s | \xi \rangle P(\xi)}{\langle \rho Y_s \rangle}. \tag{6}$$

Figure 5 shows this PDF for the ODT and DNS at six times during the simulation. At early times the soot is concentrated around $\xi = 0.4$ where the peak soot formation occurs. The soot is then transported to higher and lower mixture fractions at $14\tau_j$ and $23\tau_j$. The peak drops and the profile becomes wider. The soot is oxidized at the flame, with very little soot lean of stoichiometric. The PDF then decreases in width and the peak rises again at $\xi = 0.4$. The agreement between the ODT and DNS is very good here, with the exception of the PDF at the early $5\tau_j$

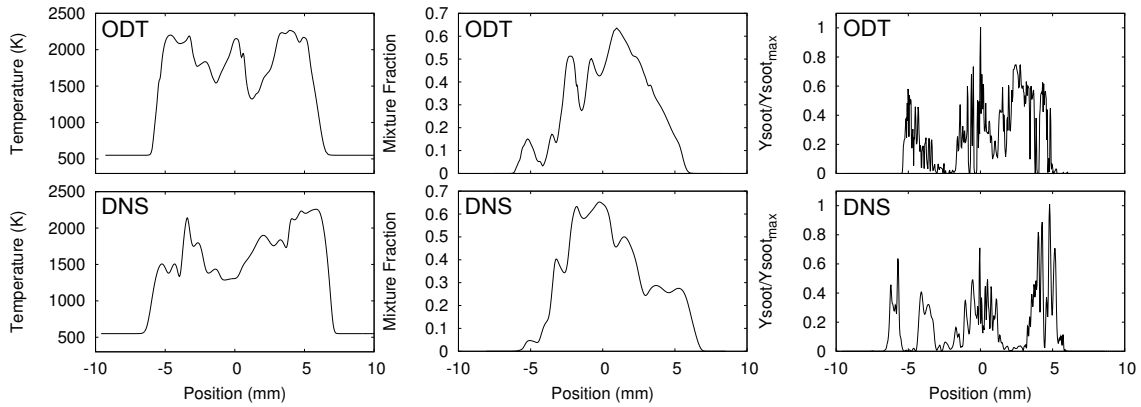


Figure 3: Representative lines of sight in the cross-stream direction (DNS) and for given realizations (ODT) at $t = 50\tau_j$.

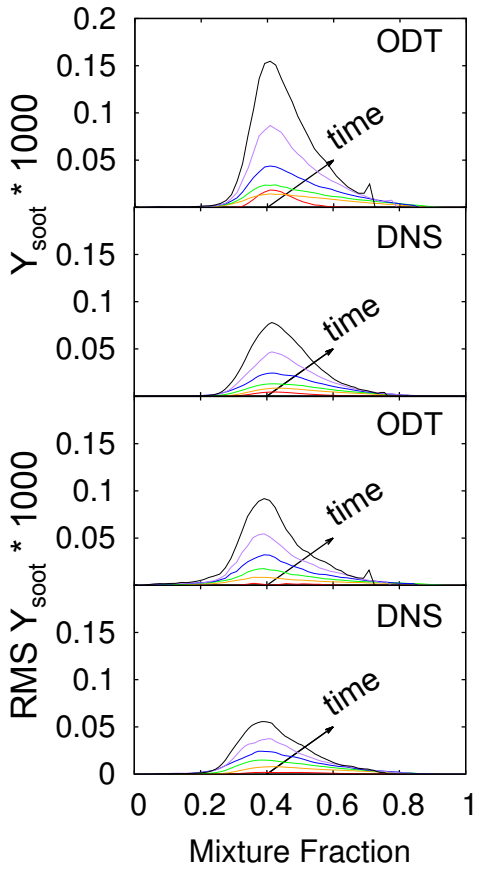


Figure 4: Conditional mean (top two) and RMS (bottom two) soot mass fractions at times of approximately 5, 14, 23, 32, 41, and 50 jet times.

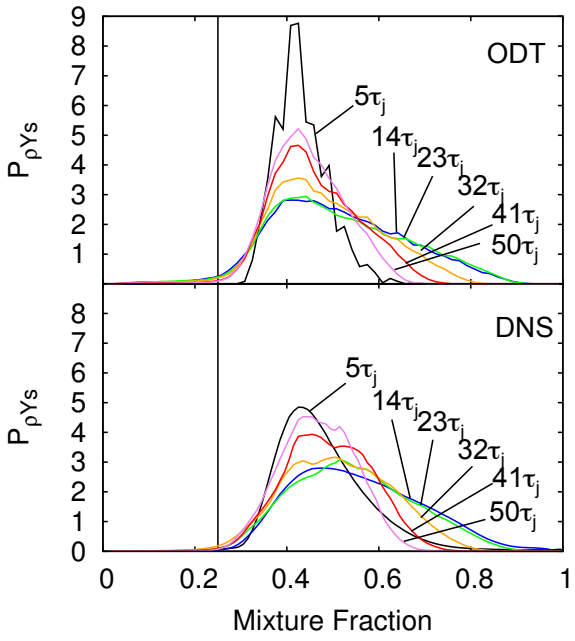


Figure 5: Soot mass weighted PDFs of mixture fraction at various times.

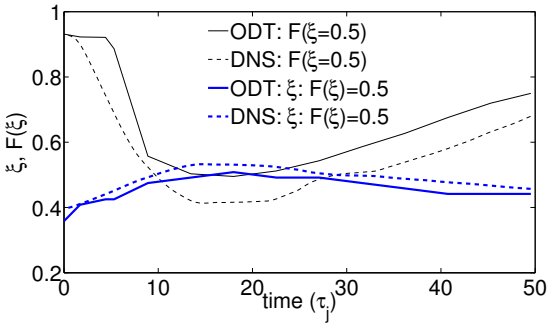


Figure 6: Fraction of soot below $\xi = 0.5$ ($F(\xi = 0.5)$, thin lines), and median mixture fraction ($\xi : F(\xi) = 0.5$, thick lines).

time, where the ODT PDF is narrower and higher than the DNS. This follows directly from the somewhat later ODT evolution of the jet, illustrated in Fig. 1.

The results in Fig. 5 are summarized in Fig. 6, which shows results of the cumulative PDF of $P_{\rho Y s}(\xi)$ defined as

$$F(\xi) = \int_0^\infty P_{\rho Y s}(\xi')d\xi'. \tag{7}$$

Two curves are shown in the figure: the fraction of the soot mass below a mixture fraction of 0.5 (the $F(\xi = 0.5)$ curves), and the median mixture fraction location where 50% of the soot mass is above and below that mixture fraction. Initially, around 90% of the soot is below $\xi = 0.5$, but quickly drops to around 45% at $14\tau_j$ as the jet mixes the soot to higher $\xi$. Afterwards, around $23\tau_j$, the soot transport is reversed to lower mixture fractions. This soot transport is similarly shown as the median mixture fraction for soot mass begins at $\xi = 0.4$, then rises to a peak around $15\tau_j$, then decreases at $23\tau_j$. In Ref. [7], this transport was analyzed in detail. There, a competition was noted between the tendency of the soot to be mixed to higher and lower mixture fractions, and the monotonic decrease in the peak mixture fraction as the fuel core is mixed out. Initially, the soot resides near its formation peak at $\xi = 0.4$ and is mixed rich and lean. But as the peak mixture fraction itself declines, the soot is squeezed back to leaner $\xi$. Eventually, the soot would be forced to cross over the stoichiometric flame where it would be oxidized, and possibly break through the flame. Figure 1 shows the centerline mean mixture fraction dropping to around 0.5 at $50\tau_j$, with the corresponding RMS mixture fraction fluctuations slightly higher than 0.1. Incidentally, the turnaround point for soot transport near $23\tau_j$ coincides in time with the location of the peak conditional scalar dissipation rate (which monotonically decreases in $\xi$ location with time) occurring at $\xi = 0.4$ [7].

The ODT shows the same behavior as the DNS with respect to this transport in the mixture fraction coordinate. The soot is transported first rich, then lean. The location of the minimum and maximum in Fig. 6 is similar for the two simulations, though the DNS pushes the soot somewhat more to rich mixture fractions than the ODT.

The mass-weighted, joint soot-mixture fraction PDFs $\tilde{P}(\xi, \rho Y_s)$ (with scaled $\rho Y_s$) are shown in Fig. 7 at $t = 50\tau_j$. Three locations are shown: (1) centerline + 2.24H, (2) centerline + 1.22H, and (3) centerline. These positions approximately yield $\xi = 0.25$, $\xi = 0.4$, and $\xi = 0.6$, respectively in the ODT simulations, and are similar in the DNS. The data are taken from a window of size 0.5H, which is 30 times the DNS grid cell size and 12% of the FWHM jet width at the given time. Only $\rho Y_s$ values greater than 0.5% of the maximum are considered, and $\rho Y_s$ values are scaled by the volume average values (1.05E-5, 2.06E-5, and 1.13E-5 for the ODT at the three positions, and 8.74E-6, 8.63E-6, and 8.24E-6 for the DNS at the three positions, respectively). The ODT and DNS agree qualitatively. At each of the three positions, there is a mixture fraction distribution due to the mixture fraction fluctuations and the finite window size used for sampling the data. At positions (1) and (3), the joint PDF peaks in the same region as the mixture fraction PDF, although there is noticeable spread in the data. There are two noticeable branches to the data, as seen at position (2). Each branch descends from the peak soot formation region at $\xi = 0.4$. The ODT data show somewhat less of the richer branch and leaner branch at positions (1) and (3), respectively, than the DNS, which, while also heavily favoring the lean and rich branches at those respective positions, also show somewhat wider distributions. Position (2) is similar for the ODT and DNS.

These PDFs are useful for understanding the soot formation process, and are also important in soot modeling. In presumed PDF approaches for use in RANS or LES (e.g., [26]), functions $F$ of the solved variables ($M_i$, $\eta_k$), such as a soot growth rate, are computed as

$$\tilde{F}(\eta_k, M_i) = \iint F(\eta_k, M_i)\tilde{P}(\eta_k, M_i)d\eta_k dM_i, \tag{8}$$

$$\approx \iint F(\eta_k, M_i)\tilde{P}(\eta_k)P(M_i)d\eta_k dM_i. \tag{9}$$

The second expression assumes independence between the soot moments and other variables—$\xi$ being one of the primary $\eta_k$ (with scalar dissipation rate, and heat loss being other common parameters). This assumption is made both for convenience, and because the joint PDF is simply not known. A common modeling assumption is to approximate $P(M_i)$ as $\delta(M_i - \overline{M}_i)$, that is, neglecting fluctuations and using the mean or filtered (solved) soot moments directly. Mueller et al. [26] present a double delta model for $P(M_i)$. Figure 7 also shows the approximation $\tilde{P}(\xi, \rho Y_s) \approx \tilde{P}(\xi)P(\rho Y_s)$ at position (2), which shows significant differences between $\tilde{P}(\xi, \rho Y_s)$ and $\tilde{P}(\xi)P(\rho Y_s)$. The joint PDF is very valuable in quantifying the effects of such modeling approximations, which are the subject of ongoing research efforts.

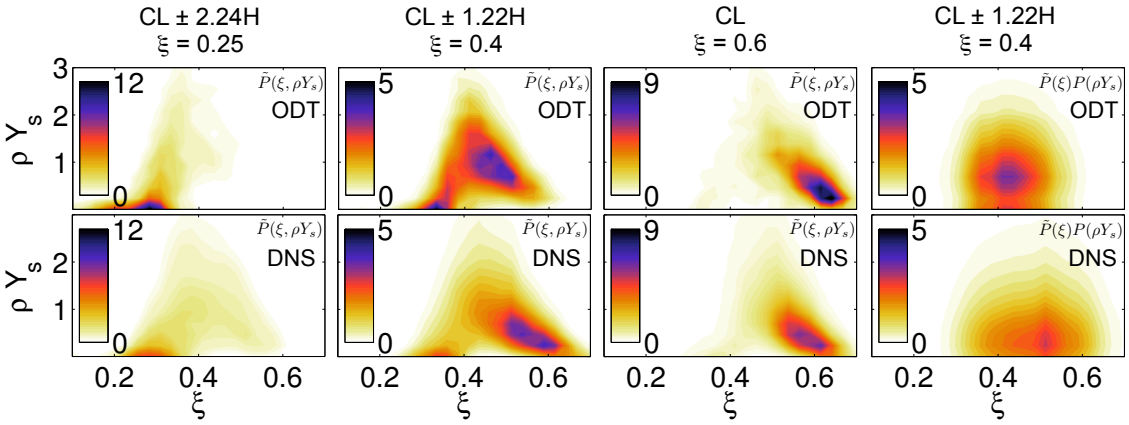


Figure 7: Joint soot, mixture fraction PDFs at three locations and the product of marginal PDFs at one location. the $\rho Y_s$ values are scaled by the average.

## 4. Conclusions

A temporally-evolving, planar, ethylene jet flame was simulated using ODT and DNS. The simulations were conducted using the same thermodynamic models, chemical kinetic mechanisms, soot models, and nearly identical transport models. This statistically one-dimensional jet configuration is ideal for comparison with the ODT model. The ODT is remarkably similar to the DNS in terms of the jet evolution, scalar profiles of temperature, mixture fraction, and soot mass fraction, and statistical quantities including mean and RMS soot concentrations, the location and transport of soot in the mixture fraction coordinate, and the joint mixture fraction-soot mass PDFs. The agreement is not perfect. At this relatively low jet Reynolds number, the scalar dissipation profile of the ODT is somewhat lower than the DNS, resulting in higher soot concentrations. In addition, the ODT is unable to capture effects of multi-dimensional flame structure, such as flame curvature. Previous work [7] considered curvature and normal strain components of the transport of soot in the mixture fraction coordinate, and showed that the mean curvature component (which ODT does not capture) is zero, while the mean normal strain component (which ODT does capture) is significant and evolves with the evolution of the mixture fraction profile, which the ODT captures well. Qualitative agreement is very good and the behavior of the soot is the same in the ODT and DNS as presented. This is significant considering the computational cost differences in the simulations. Used in conjunction with experiments and/or with DNS, or validated with DNS under certain conditions, ODT could be used to study turbulent soot formation with parametric variations in parameters and under other conditions that are costly for DNS, such as long run times, high Reynolds numbers, and optically thick domains. Such study would provide detailed soot-flame structure, and numerical data for model development and validation.


[1] U.S. Environmental Protection Agency, Air quality criteria for particulate matter, EPA/600/P-99/002aF, October 2004.

[2] H. Bockhorn, Soot formation in combustion, Springer-Verlag, Heidelberg, Germany, 1994.

[3] D. O. Lignell, J. H. Chen, P. J. Smith, T. Lu, C. K. Law, The effect of flame structure on soot formation and transport in turbulent nonpremixed flames using direct numerical simulation, Combustion and Flame 151 (2007) 2–28.

[4] J. H. Kent, D. Honnery, Soot and mixture fraction in turbulent diffusion flames, Combustion Science and Technology 54 (1987) 383–397.

[5] C. S. Yoo, H. G. Im, Transient soot dynamics in turbulent nonpremixed ethylene-air counterflow flames, Proceedings of the Combustion Institute 31 (2007) 701–708.

[6] F. Bisetti, G. Blanquart, M. Mueller, H. Pitsch, On the formation and early evolution of soot in turbulent nonpremixed flames, Combustion and Flame 159 (2012) 317–335.

[7] D. O. Lignell, J. H. Chen, P. J. Smith, Three-dimensional direct numerical simulation of soot formation and transport in a temporally-evolving nonpremixed ethylene jet flame, Combustion and Flame 155 (2008) 316–333.

[8] A. Attili, F. Bisetti, M. E. Mueller, Dns of soot formation and growth in turbulent non-premixed flames: Damköhler number effects and lagrangian statistics of soot transport, in: Center for Turbulence Research, Proceedings of the Summer Program, 2012.

[9] A. R. Kerstein, One-dimensional turbulence: model formulation and application to homogeneous turbulence, shear flows, and buoyant stratified flows, Journal of Fluid Mechanics 392 (1999) 277–334.

[10] E. Gonzalez-Juez, R. Schmidt, A. Kerstein, ODTLES simulations of wall-bounded flows, Physics of Fluids 23 (2011) 125102.

[11] T. Echekki, A. R. Kerstein, J. C. Sutherland, The one-dimensional-turbulence model, in: T. Echekki, E. Mastorakos (Eds.), Turbulent Combustion Modeling: Advances, New Trends, and Perspectives, Springer-Verlag, Heidelberg, Germany, 2011, pp. 249–276.

[12] T. Echekki, A. R. Kerstein, T. D. Dreeben, One-dimensional turbulence simulation of turbulent jet diffusion flames: model formulation and illustrative applications, Combustion and Flame 125 (2001) 1083–1105.

[13] J. C. Hewson, A. R. Kerstein, Local extinction and reignition in nonpremixed turbulent $CO/H_2/N_2$ jet flames., Combustion Science and Technology 174 (2002) 35–66.

[14] N. Punati, J. C. Sutherland, A. R. Kerstein, E. R. Hawkes, J. H. Chen, An evaluation of the one-dimensional turbulence model: Comparison with direct numerical simulations of $CO/H_2$ jets with extinction and reignition, Proceedings of the Combustion Institute 33 (2011) 1515–1522.

[15] D. O. Lignell, D. Rappleye, One-dimensional-turbulence simulation of flame extinction and reignition in planar ethylene jet flames, Combustion and Flame 159 (2012) 2930–2943.
[16] A. J. Ricks, J. C. Hewson, A. R. Kerstein, J. P. Gore, S. R. Tieszen, W. T. Ashurst, A spatially developing one-dimensional turbulence (ODT) study of soot and enthalpy evolution in meter-scale buoyant turbulent flames, Combustion Science and Technology 182 (2010) 60–101.
[17] A. R. Kerstein, Linear-eddy modelling of turbulent transport. part 6. microstructure of diffusive scalar mixing fields, Journal of Fluid Mechanics 231 (1991) 361–394.
[18] J. H. Chen, A. Choudhary, B. de Supinski, M. DeVries, E. R. Hawkes, S. Klasky, W. K. Liao, K. L. Ma, J. Mellor-Crummey, N. Podhorszki, R. Sankaran, S. Shende, C. S. Yoo, Terascale direct numerical simulations of turbulent combustion using S3D, Computational Science and Discovery 2 (2009) 1–31.
[19] R. J. Kee, F. M. Rupley, J. A. Miller, Chemkin, Reaction Design, Inc., San Diego CA (2000).
[20] R. J. Kee, G. Dixon-Lewis, J. Warnatz, M. E. Coltrin, J. A. Miller, H. K. Moffat, Transport, Reaction Design, Inc., San Diego CA (2000).
[21] D. O. Lignell, Direct numerical simulation of soot formation in nonpremixed, turbulent ethylene flames, Ph.D. thesis, University of Utah (2008).
[22] K. M. Leung, R. P. Lindstedt, A simplified reaction mechanism for soot formation in nonpremixed flames, Combustion and Flame 87 (1991) 289–305.
[23] D. O. Lignell, A. R. Kerstein, G. Sun, E. I. Monson, Mesh adaption for efficient multiscale implementation of one-dimensional turbulence, Theoretical and Computational Fluid Dynamics 27.
[24] D. Goodwin, Cantera, an object-oriented software toolkit for chemical kinetics, thermodynamics, and transport processes, `http://code.google.com/p/cantera` (August 2011).
[25] S. B. Pope, Turbulent Flows, Cambridge University Press, New York, 2000.
[26] M. E. Mueller, H. Pitsch, Large eddy simulation subfilter modeling of soot-turbulence interactions, Physics of Fluids 23 (2011) 115104.